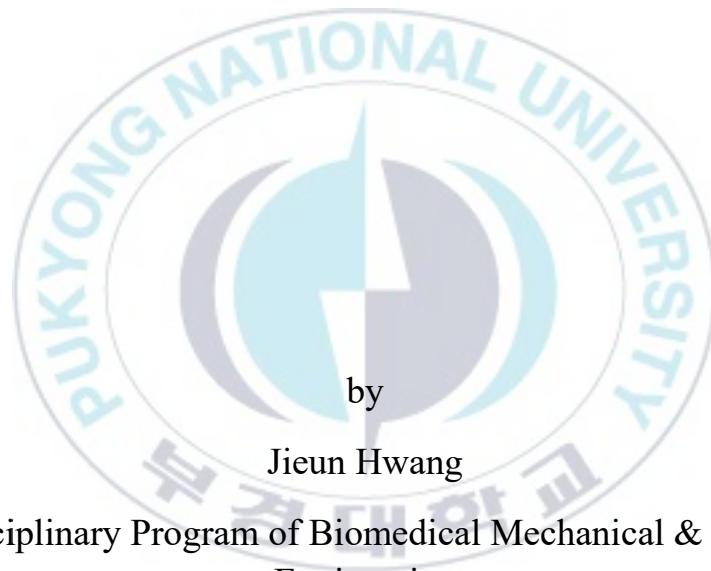Thesis for the Degree of Master of Engineering

Dual-wavelength-assisted photocoagulation effects for hemostasis of benign prostate hyperplasia

by

Jieun Hwang

Interdisciplinary Program of Biomedical Mechanical & Electrical Engineering

The Graduate School

Pukyong National University

February 2019

Dual-wavelength-assisted photocoagulation effects for hemostasis of benign prostate hyperplasia

전립선 비대증 지혈을 위한 다파장 레이저 응용 광응고 효과 연구

Advisor: Prof. Hyun Wook Kang

by

Jieun Hwang

A thesis submitted in partial fulfillment of the requirements
for the degree of

Master of Engineering in Department of Spatial Information Engineering,

The Graduate School,

Pukyong National University

February 2019

Dual-wavelength-assisted photocoagulation effects for hemostasis of benign prostate hyperplasia
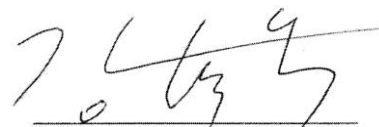
A dissertation

by

Jieun Hwang

Approved by:

_____

(Chairman) Junghwan Oh Ph. D

_____
(Member) Sung-won Kim M. D

_____
(Member) Hyun Wook Kang Ph. D

February 23, 2019

Dual-wavelength-assisted photocoagulation effects for hemostasis of benign prostate

hyperplasia

Jieun Hwang

Interdisciplinary Program of Biomedical Mechanical & Electrical Engineering

The Graduate School

Pukyong National University

Abstract

전립선 비대증은 전립선의 비대로 인한 요로의 막힘에 의해 소변량의 감소 및 전립선의 간질 세포나 상피 세포의 증가를 포함하는 비뇨기과 질병이다. 비대해진 전립선은 요도 폐색, 요실금, 잦은 배뇨, 배뇨 장애, 야뇨증의 원인이 된다. 전립선 비대증 치료를 위한 다양한 저 침습 수술 중 레이저 전립선 절제술은 빠른 증상 완화와 낮은 부작용 발생으로 효율성을 인정을 받고 있다. 다양한 파장대의 레이저가 임상에서 사용되고 있는데, 그 중 조직의 제거나 응고(980, 1064 nm), 증발(532 nm), 적출(1470, 2000, 2120 nm)등과 같이 제공되는 파장에 따라서 다양한 수술적 기술을 개발할 수 있다. 그리고 532 nm 레이저는 높은 광 흡수율과 효과적인 전립선 조직 제거로 임상에서 인정받고 있다. 그러나 큰 조직을 제거 할 경우 동맥이나 정맥의 출혈로 인하여, 방광경 촬영 시 수술자의 시야에 영향을 주며 그로 인해 수술 시간에 영향을 가져올 수 있다. 레이저 전립선 절제술을(532 nm) 이용해서 큰 조직을 제거하는 경우 높은 에너지를 이용하기 때문에 수술 도중 출혈이 발생하는 확률은 10 % 다다른다. 게다가 혈관 계통에 높은 흡수율을 가진 532 nm 파장대의 레이저는 광침투 깊이가 짧기 때문에, 깊은

광침투력을 가진 980 nm 파장의 레이저는 보다 깊은 곳에서 발생하는 출혈을 효과적으로 제어 해 줄 수 있다. 따라서, 본 연구에서는 효과적인 레이저 전립선 절제를 위해 두 가지 파장의 레이저를(980,532 nm) 결합하여 광응고 효과의 개선과 그 가능성을 조사하였다. 두 가지 파장을 이용한 지혈 효과 및 광 반응의 생체 외 조직 실험과 생체 내 실험을 통해 광응고 효과 및 지혈 효과를 각각 확인할 수 있었다. 결과적으로 다파장 레이저를 이용한 전립선 비대증 치료는 출혈을 효과적으로 지혈 할 수 있는 방법이 될 수 있다.

Table of contents

List of figures

1. Introduction

1.1. Benign prostatic hyperplasia

Benign prostate hyperplasia (BPH) is a urological disease involving enlargement of epithelial and stromal cells in the transition zone of the prostate, resulting in annual 1.2 million surgical procedures. The enlarged prostate causes obstructive urination, accompanying urge incontinence, frequent urination, dysuria, and nocturia [2]. The untreated BPH adversely affect quality of life in association with various complications such as urinary retention, urinary tract infections, bladder impairment, and kidney disease. Among various minimally-invasive surgical treatments for BPH, laser prostatectomy has gained a great attention due to rapid relief of symptoms and low risk of side-effects [3]. A number of wavelengths have been clinically investigated and utilized, including 532, 980, 1064, 2000, and 2120 *nm* [4]. Depending on the applied wavelength, different surgical techniques have thus been developed such as ablation/coagulation (980 and 1064 *nm*), vaporization (532 *nm*), and enucleation (2000 and 2120 *nm*) [4].

1.2. Overview of photothermal therapy for BPH

Among various wavelengths for laser prostatectomy, a wavelength of 532 *nm* has been clinically accepted to vaporize prostatic tissue in an effective and rather hemostatic

manner on account of high light absorption by vasculature [5]. However, bulky tissue vaporization sometimes encounters venous or arterial bleeding, impairing cystoscopic visibility and eventually protracting operation time. Reportedly, the incidence rate of intraoperative bleeding reached up to 10% during 532-nm laser prostatectomy [6]. In particular, laser power has recently been increased up to 180 W to rapidly debulk a large size of prostate glands, which can accompany a high probability of bleeding during the vaporization procedure [1, 5]. Although small blood vessels or mucosal veins can readily be coagulated with laser light and irrigation fluid, management of the arterial bleeding still remains rather challenging to achieve the complete hemostasis. Typically, upon encountering the arterial bleeding during the laser prostatectomy, urological surgeons increase the distance between the fiber tip and the bleeding site (3~4 mm) and/or decrease the laser power to reduce the irradiance below vaporization threshold [7]. Then, the urologists start to sweep the laser light at a fast speed by circling the beam around the bleeder as the bleeding vessel has a circular shape [8, 9]. Another approach to manage the bleeding is to improve visibility by using an irrigation pump [7] and to compress the bleeder by using a beak of the cystoscope [9]. If all the measures fail to achieve hemostasis, an electrocautery loop can be inserted through the cystoscope to cope with the bleeding site [7-9]. However, in spite of the hemostatic capability, using the electrode can prolong the procedure due to device replacement and can even cause significant thermal injury to the adjacent tissue. As a result, the undesirable tissue coagulation can result in dysuria post-operatively [7, 10]. Thus, more effective approach is still required to accomplish the complete hemostasis during the

2

532-nm laser prostatectomy.

1.3. Overview of hemostasis effect using laser

A number of studies have demonstrated hemostatic features of laser application during surgery. Argon (480~520 nm) and Nd:YAG (1064 nm) lasers have clinically been used to photocoagulate the bleeding peptic ulcers in an endoscopic manner [11, 12]. Due to thermal interactions, the light manages the bleeders limitedly from small arteries (0.25-mm in diameter). A potassium-titanyl-phosphate (KTP, 532 nm) laser was evaluated as a feasible hemostatic cutting tool for laparoscopic partial nephrectomy in a porcine model [13, 14]. Strong light absorption by hemoglobin yielded a large coagulation depth in the kidney tissue. However, frequent blood carbonization and smoke formation caused the minimal capability to stop bleeders during the laparoscopic procedure. Moreover, kidney mainly consists of glandular tissue (i.e., minimal collagen), which is quite difficult to physically seal off the bleeding sites in terms of thermal denaturation. A diode laser (1470 nm) was used to seal blood vessels for hemostasis through thermal fusion [15-17]. *Ex vivo* and *in vivo* results well demonstrated the feasibility of the infrared light for rapid sealing of the blood vessels in air. However, the hemostatic capability of the 532-nm wavelength for BPH treatment particularly in saline environment still remains unexplored. In addition, high absorption of vasculature at 532 nm yields a short optical penetration of ~0.8 mm in soft tissue [18].

Thus, the wavelength was difficult to achieve hemostasis on the relatively deep bleeding sites. In order to overcome the current limitation, a clinically available infrared wavelength (980 nm) with a deeper optical penetration depth (5 mm) can be combined with the visible wavelength (532 nm) for the eventual control of the deep bleeders [18].

2. Photocoagulation effects for *ex vivo* thermal hemostasis

2.1. Purpose

The purpose of the current study was to investigate the feasible thermal effects of the two combined wavelengths (532 and 980 nm) on the enhanced photocoagulation for the laser prostatectomy. It was hypothesized that the dual-wavelengths with different optical characteristics could augment the spatial extent of the irreversible thermal coagulation on the bleeding sites, leading to the complete hemostasis during the 532-nm laser prostatectomy. Since the previous perfused kidney model suffers from lack of collagen (unlike prostate consisting of glandular and stromal tissues [19]), a new perfused skin phantom model was developed instead for reliable and quantitative evaluations on various irradiation conditions. The features of thermal hemostasis during the laser irradiation were thus examined and monitored in terms of coagulation time and tissue responses.

2.2. Materials and Methods

2.2.1. Kidney tissue preparation

Porcine kidney was used for pre-screening experiments to identify the potential

irradiation conditions for thermal hemostasis. The tissues were harvested from a local abattoir, prepared in size of in 3×3 cm^2, and stored in saline at 4 ˚C to prevent dehydration and structural deformation.

2.2.2. Ex vivo kidney tissue testing

During *ex vivo* experiments, each sample was situated in a customized tissue holder filled with saline and covered with an aluminum plate with an aperture (1.5×1.5 cm^2) at the center. Laser light was irradiated merely on the tissue surface that was exposed through the aperture and was used to create two 1.5-cm long coagulation lines (5 mm apart) in each tissue sample. **Figure 1(a)** shows a schematic diagram of the *ex vivo* experimental set-up. Due to availability of commercial systems for laser prostatectomy, two wavelengths were tested for the current study: quasi-cw Q-switched 532 nm (100 ns at 20 kHz; GreenLight XPS, Boston Scientific, Corp., San Jose, CA) and customized cw 980 nm (similar specifications to those of clinical laser [18]). Each wavelength was delivered through a 600-µm multimode core-diameter fiber. The distal ends of both the fibers were tilted at 23 and –23 degrees for 532 and 980 nm, respectively. Working distance (between fiber tips and tissue surface) of 3 mm and treatment speed of 4 mm/s was selected for the current study in order to emulate clinical conditions [20]. Thus, the irradiation time for each coagulation line was 3.75 s (= 1.5 cm / 4 mm/s). A XY translational stage was used to control the movement of each sample (i.e., 4 mm/s) to create the two 1.5-cm coagulation lines (5 mm apart along y-axis) on the tissue surface.

The preliminary testing confirmed that both the fibers had the equivalent (overlapped) size of the beams spot (i.e., 1.5 mm in diameter) on the surface. During the tests, saline was constantly supplied at 4.4 ml/min to the irradiated spot for cleaning and cooling. The tested power conditions for each wavelength ranged from 10 to 40 W with a 5-W increment. Five different irradiation modes were tested: 532 nm only, 980 nm only, sequential applications (532→980 nm and 980→532 nm), and dual-wavelength (i.e., simultaneous irradiation of 532 and 980 nm). For the sequential applications, it took approximately 5 s to switch one wavelength to the other to irradiate along the same path. Each condition was repeated five times ($N = 5$). To explore the optimal conditions for photocoagulation, all the tested tissues were evaluated in light of spatial extent of coagulation. Initially, each tested tissue was frozen at -80 ˚C and then cross-sectioned by 1-mm thickness (total ten specimens) with a razor blade. All the cross-sections were photographed by using a digital camera. Image J (National Institute of the Health, Bethesda, Maryland) was implemented to measure the degree of the irreversible thermal coagulation. For the current study, the coagulation region was defined as the discolored area (tan color) in the treated tissue. Thus, the coagulation depth was measured from the top to the bottom of each discolored area while the coagulation width was determined as the discolored width only at the tissue surface. The coagulation volume was calculated by integrating a series of the coagulation areas measured from the ten cross-sections. To assess the spatial distribution of the coagulation in the tissue, non-dimensional aspect ratio (AR) was also estimated by dividing the coagulation depth by the width. As the purpose of the study was to assess

the hemostatic effect of the dual-wavelength irradiation, no tissue ablation was considered for quantitative analysis.

2.2.3. Perfused bleeding tissue phantom preparation

Figure 1(b) demonstrates an experimental set-up for perfused skin phantom testing with the pre-identified photocoagulation conditions from kidney testing (20 W for 532 nm and 40 W for 980 nm; working distance = 3 mm; beam diameter = 1.5 mm). The corresponding irradiances for 532 and 980 nm were 11.1 and 22.2 W/mm^2, respectively. In spite of no direct relation to urological tissue, the skin phantom was developed to reflect the main component of prostate (i.e., collagenous stromal tissue). Additionally, the developed model could provide the bleeding environment to evaluate various photocoagulation methods in a reliable and quantitative manner. For the phantom preparation, porcine skin (consisting of epidermis, dermis, and subcutaneous fat) was initially harvested and prepared in size of 3×3 cm^2. A 1-cm long wound was initially created on the skin (deep down to subcutaneous layer) by using a razor blade. To emulate a blood vessel underneath the skin (i.e., 1 mm subsurface), a channel (around 2 mm in diameter) was drilled in the subcutaneous layer until it encountered the vertical wound cut from the surface. Then, a plastic tube (2.7 mm in outer diameter) was connected (1~2 mm) to the channel entrance in the tissue, and the other end of the tube was connected to the syringe pump (NE-3001, New Era Pump Systems, NY, USA). No physical interaction was confirmed between the incident laser light and the connecting

tube during the tests. The pump was employed to perfuse the heparinized rabbit blood at a flow rate of 0.5 ml/s through the channel to the wound to emulate tissue bleeding during laser prostatectomy. Once the bleeding was initiated from the wound at a rate of 4.2 ± 0.5 ml/min, laser beam was moved in a zigzag pattern (dotted lines) and covered the entire wound length as shown in **Figure 1(b)** in an attempt to achieve thermal hemostasis.

2.2.4. Perfused tissue phantom testing

Unlike the kidney testing (4 mm/s), the treatment speed for the phantom testing was reduced to 1 mm/s as the skin tissue has higher thermal resistance than the kidney tissue had [21], which was also confirmed by the preliminary testing. For a single zigzag pattern, the beam spot was initially moved by 2 mm at the speed of 1 mm/s along the x-axis (from left to right) and then by 2 mm at 2 mm/s along the y-axis (from top to bottom). The single pattern was thus repeated eight times to cover the entire bleeding wound (i.e., reversing direction along x-axis per pattern; **Figure 1(b)**), and the total irradiation time was 24 s (= 3 s for each pattern $\times$ 8 repetitions). Three different irradiation modes were tested for the perfused phantom testing: 532 nm only, 980 nm only, and dual-wavelength. In turn, the total energy density (J/mm^2) corresponded to 266.4, 532.8, and 799.2 J/mm^2, respectively. The entire irradiation process was recorded to quantify the overall photocoagulation time. Probit analysis was used as a probabilistic (binary) approach to estimate the complete hemostasis time with a 50 % probability [22]. Thus, 1 is considered hemostasis whereas 0 non-hemostasis. All the

conditions were repeated five time ($N = 5$). After the laser treatment, the top surface of each sample was imaged by using a digital camera. Each treated tissue was then fixed in formalin and prepared for histological analysis. All the histology slides were stained with hematoxylin and eosin (HE) to assess the extent of the irreversible thermal coagulation in the phantom tissue. From each histology slide, the coagulation depth and width were defined as the distance between top and bottom of the coagulated area and the overall spatial extent of the coagulated region at the surface level, respectively.

2.2.5. Statistical analysis

For statistical analysis (unpaired data), Mann Whitney U test was performed as a non-parametric method on all the measured coagulation depth, width, and volume, and $p < 0.05$ represents statistical significance.
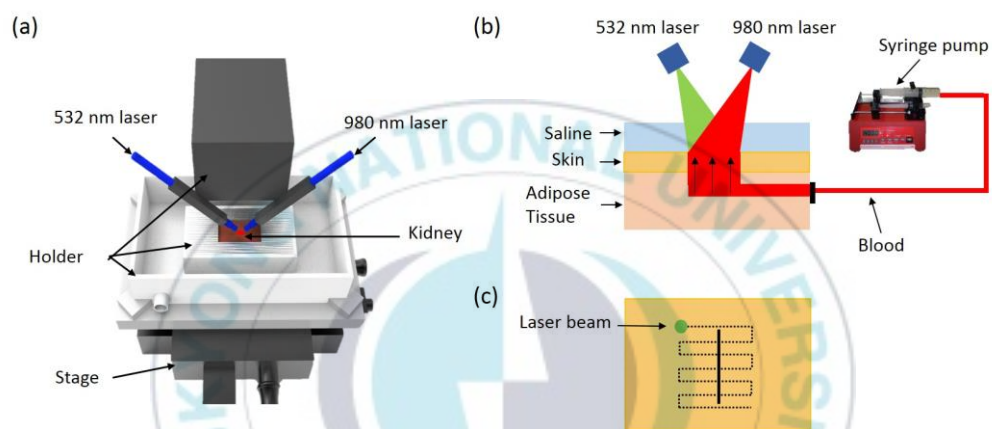
Figure 1. Experimental set up for dual wavelength photocoagulation: (a) ex vivo

kidney testing and (b), (c) perfused tissue phantom testing

2.3. Results and Discussion

2.3.1. Thermal coagulation in kidney tissue

Figure 2 characterizes the spatial distribution of the irreversible thermal coagulation in kidney tissue (straight lines) at various power levels for two individual wavelengths. **Figures 2(a) and 2(b)** represent coagulation depth and width, respectively. The power levels were merely associated with the coagulative process (no ablation was included). Regardless of the wavelength, the coagulation features increased linearly with the applied power. Overall, 532 nm initiated the tissue coagulation at lower power, compared with 980 nm. At the same power of 20 W, the 532 nm created 1.5-fold deeper (1.37 ± 0.13 mm) and 2.2-fold wider (2.04 ± 0.19 mm) coagulation regions than the 980 nm did (0.91 ± 0.12 mm for depth and 0.91 ± 0.21 mm for width; $p < 0.001$). In fact, the 532-nm yielded increased rates per unit power of 0.08 mm/W for the depth and 0.12 mm/W for the width, which was 1.6- and 2.4-fold higher than those of the 980 nm (i.e., 0.05 mm/W for depth and 0.05 mm/W for width; $p < 0.001$). To maximize the degree of the thermal coagulation in the tissue, the maximal laser power levels were selected for the rest of the study (i.e., 20 W for 532 nm and 40 W for 980 nm). In turn, each wavelength was able to generate the coagulation depth of ~1.3 mm and the width of 1.8~2 mm in the kidney tissue.

Figure 3 shows the effect of various irradiation combinations on coagulation characteristics in porcine kidney (straight lines). The applied power levels for 532 and

980 nm were 20 and 40 W, respectively. In the case of coagulation depth in **Figure 3(a)**, dual-wavelength created up to 1.4-fold deeper coagulation regions than other conditions ($p < 0.001$). The other conditions (532 nm, 980 nm, 532→980 nm, and 980→532 nm) induced the comparable coagulation depths (1.30~1.37 mm; p = 0.47~0.18). On the other hand, the coagulation width in **Figure 3(b)** demonstrated that both the sequential and the dual-wavelength irradiations were associated with the wider coagulation regions than either the 532 nm or the 980 nm did (around 2.5 mm for sequential and dual vs. 2.00 ± 0.19 mm for 532 nm and 1.62 ± 0.20 mm for 980 nm; p < 0.001). Among the combinations, the 980-nm wavelength generated the narrowest coagulation region whereas the dual-wavelength resulted in the largest degree of the irreversible tissue coagulation.

Figure 4(a) displays cross-sectional images of porcine kidney tissue after laser coagulation. The white dotted lines represent the region of the coagulated tissue. Similar to **Figure 3**, dual-wavelength created the largest coagulation area (36.3 ± 5.0 mm^2; up to 2.3 times larger) than other irradiation modes did ($p < 0.001$). Two sequential modes (532→980 nm and 980→532 nm) yielded an almost equivalent size of the coagulation area (p =0.47). **Figure 4(b)** represents the quantified coagulation volume (left axis; bar) and non-dimensional AR (right axis; red line) for various irradiation modes. Correspondingly, the coagulation volume was developed in the order of the dual-wavelength, the sequential modes, the 532 nm, and the 980 nm. The dual-wavelength created an up to 2.5-fold larger coagulation volume than the other conditions did ($p < 0.001$). In the case of AR, the simultaneous irradiation of the two

wavelengths entailed a 20% larger AR than the sequential irradiations did, representing the deeper penetration of the thermal coagulation into the tissue. On the other hand, the 980 nm generated relatively deeper and narrower coagulation areas.

## 2.3.2. Thermal coagulation on perfused skin phantoms

Figure 5 shows the images of thermal coagulation on perfused skin phantoms with three different irradiation modes (532 nm, 980 nm, and dual-wavelength) captured at two different times. Initially, significant bleeding was confirmed at the wound site prior to laser irradiation (pre-treatment in top images; **Figure 5(a)**). However, 15 s after the irradiation (bottom images), the disappearance of bleeding vividly evidenced that the application of the dual-wavelength coagulated the wound site and eventually achieved the complete hemostasis post-irradiation (i.e., clear color in far-right bottom image; **Figure 5(a)**). Neither the 532 nor the 980 nm completely stopped the bleeders as the bleeding continued at the wound (i.e., red color in far-left and middle bottom images; **Figure 5(a)**). In fact, due to the substantial bleeding, the wound was almost invisible. It should be noted that both the 532 nm and the dual images seemed purplish as a 532-nm filter was used to prevent any optical damage to a digital camera during the irradiation. **Figure 5(b)** demonstrates the Probit analysis of the coagulation times for the three irradiation modes. Binomial responses represent no hemostasis (0) and complete hemostasis (1). According to the results, the dual-wavelength (solid line) was able to discontinue the bleeding within approximately 11 s after the onset of the laser

14

irradiation. On the other hand, both the 532 and the 980 nm (dotted lines) were unable to obtain the thermal coagulation, given the experimental conditions.

Figure 6(a) exhibits the captured images of the tissues after photothermal coagulation (top: tissue surface and bottom: histology images of cross-sections). Top images present the laser-induced discoloration on the tissue surface along the pre-created wound (horizontally positioned). 532 nm demonstrated a very thin discoloration around the bleeding wound whereas 980 nm was associated with a discernably thick coagulation line. Contrary to the application of a single wavelength (532 or 980 nm), the dual-wavelength irradiation yielded the widest lateral discoloration on the surface (~3 mm in vertical direction). Histological images (bottom) validated that the dual-wavelength covered the entire bleeding site in terms of a larger area of coagulation (orange dotted lines). Unlike kidney testing (Figure 4), the 532 nm yielded relatively superficial coagulation whereas the 980 nm created a deeper and wider coagulation region than the 532 nm did. Figure 6(b) quantifies the degree of the tissue coagulation for all the tested conditions from the histology images. The dual-wavelength irradiation entailed a more than 4-fold deeper coagulation than the 532 nm did ($p < 0.001$) but a similar coagulation depth to that of the 980 nm ($p = 0.20$). The coagulation width of the dual-wavelength was up to 3-fold wider than those of the other wavelengths ($p < 0.001$).

2.3.3. Numerical simulations of temperature distribution in kidney tissue

Figure 7 demonstrates comparison of temperature distributions for three different conditions (20-W 532 nm, 40-W 980 nm, and 60-W dual-wavelength). The black dashed lines represent the threshold temperature (333 K) for tissue coagulation [24]. Due to application of the lower power and strong scattering features, the 532-nm wavelength yielded a shallow but wide temperature distribution. On the other hand, the 980-nm wavelength created a deep but narrow temperature distribution on account of a deep optical penetration depth along with less scattering effect. Compared with the single wavelengths, the dual-wavelength with higher laser power generated a higher surface temperature (i.e., 110 ˚C for dual vs. 72 ˚C for 532 nm and 64 ˚C for 980 nm).
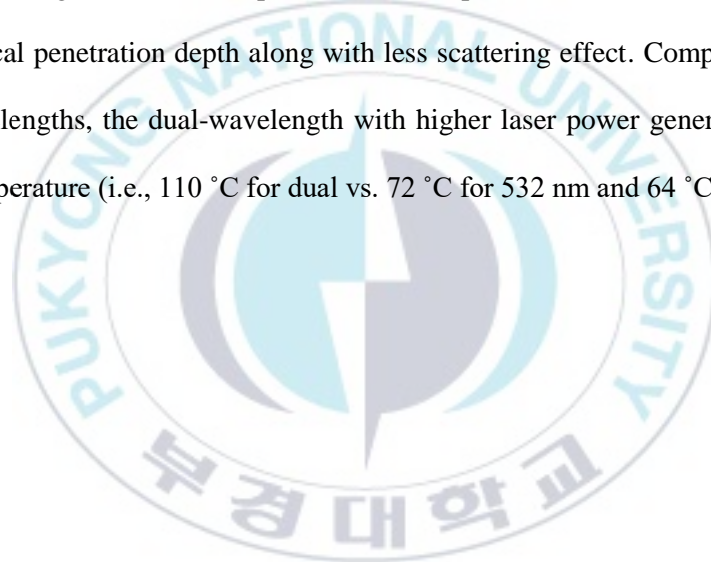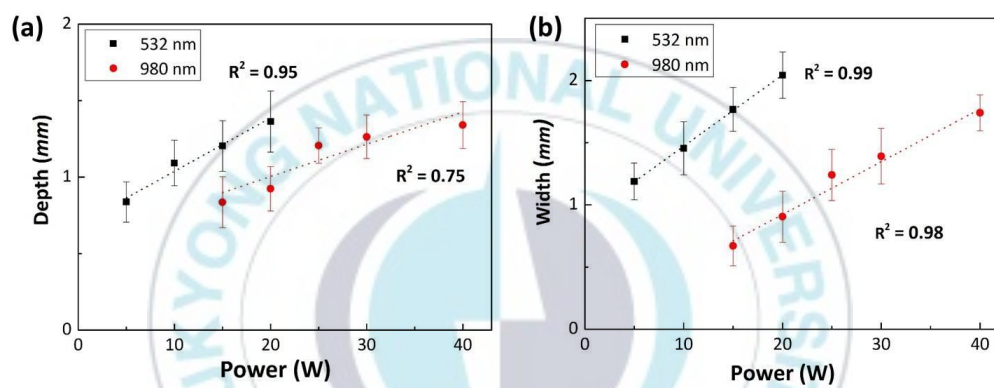
Figure 2. Comparison of coagulation characteristics between 532 (black square) and
980 nm (red circle): (a) coagulation depth and (b) coagulation width
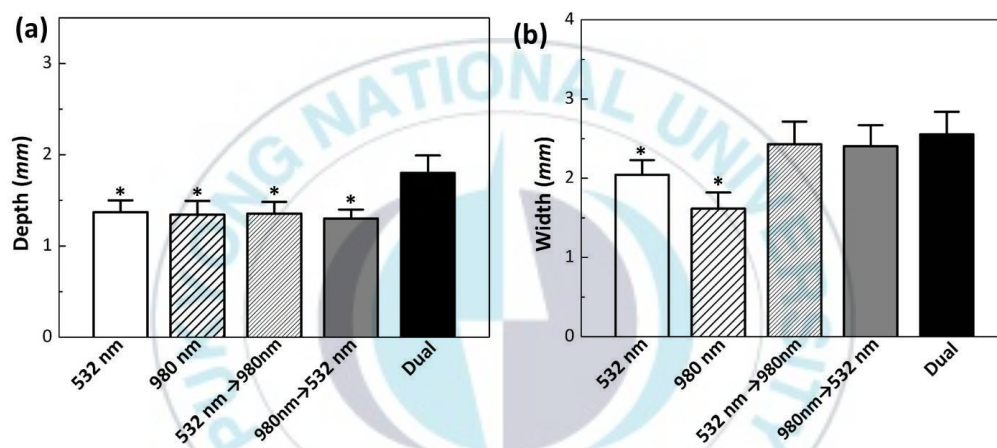
Figure 3. Comparison of various irradiation modes: coagulation (a) depth and (b) width. Note that 20 and 40 W were used for 532 and 980 nm, respectively ($N = 5$; *: $p < 0.001$ vs. dual).
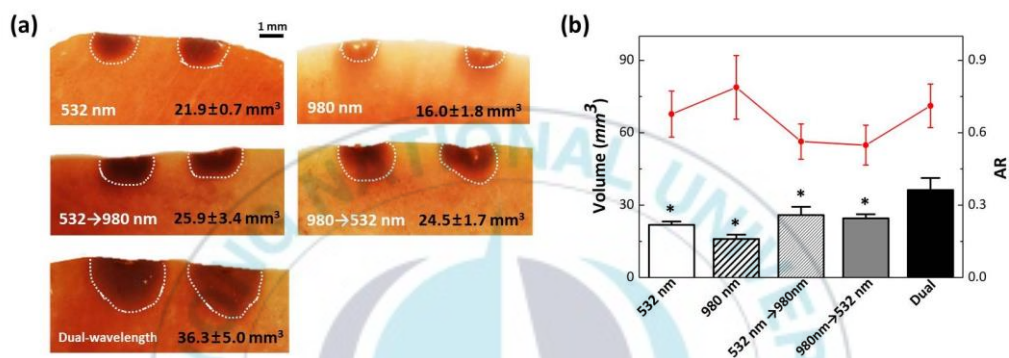
Figure 4. Effect of irradiation modes on thermal coagulation: (a) cross-sectional images of coagulated tissue and (b) coagulation volume (bar; left axis) and aspect ratio (AR, red lines; right axis). Note that the number at the right corner in each image represents the measured coagulation area ($N = 5$; Bar = 1 mm; *: $p < 0.001$ vs. dual).
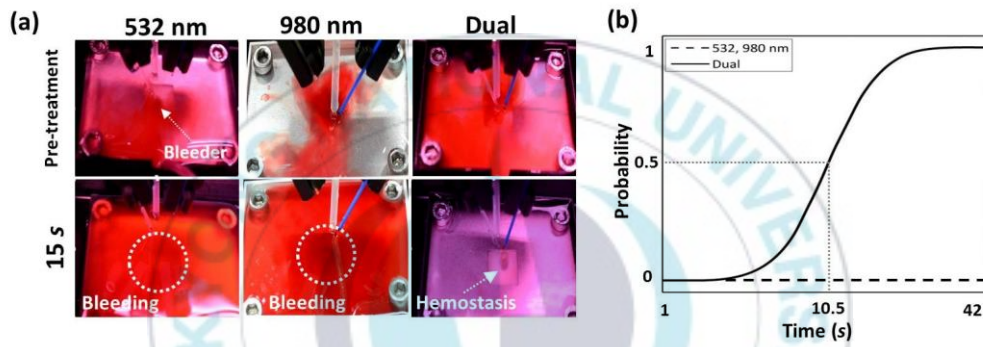
Figure 5. Photocoagulation on perfused tissue phantoms: (a) captured images under three irradiation modes (left column= 532 nm, middle column = 980 nm, and right column = dual-wavelength) at various times (top = pre-irradiation and bottom = 15 s after irradiation) and (b) Probit analysis on coagulation time
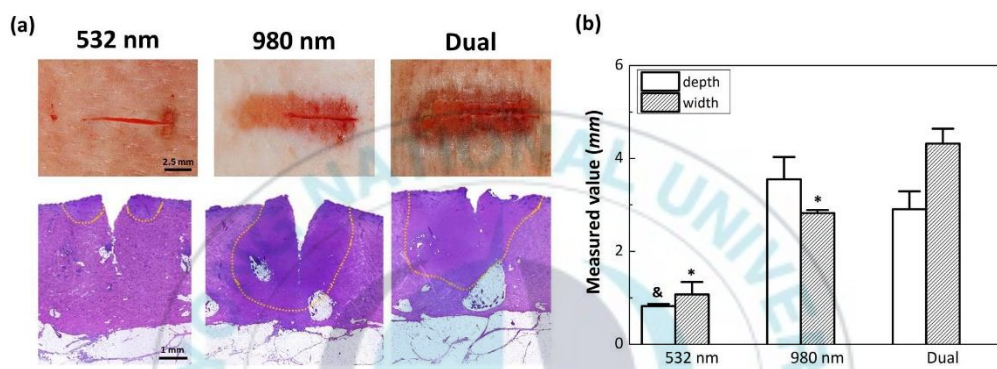
Figure 6. Coagulated tissue after thermal hemostasis at three different conditions (532 nm, 980 nm, and dual-wavelength): (a) surface images (top) and histology (bottom; 40×) and (b) measured coagulation ($N = 5$; &: $p < 0.001$ vs. dual and *: $p < 0.001$ vs. dual).
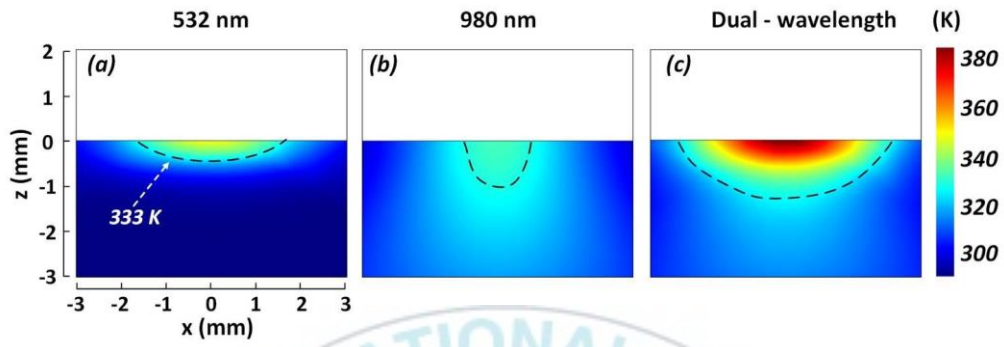
Figure 7. Numerical simulations of temperature distribution in kidney tissue under various irradiation conditions: (a) 532 nm (20 W), (b) 980 nm (40 W), and (c) dual-wavelength (20-W 532 nm and 40-W 980 nm)

3. Hemostatic effects depending on the urological tissue and blood vessels in *in vivo*

3.1. Purpose

In the previous study, dual wavelength has demonstrated the feasibility of the enhanced thermal hemostasis in *ex vivo* tests. Based upon the ex vivo test, we performed in vivo kidney testing and in vivo ear testing to check hemostasis possibility. Firstly, we conducted rabbit kidney test for possibility of hemostasis using dual-wavelength laser that confirmed by *ex vivo* hemostasis test. The aim of the kidney bleeding model test was to validate the hemostatic effect of the dual wavelengths on *in vivo* kidney tissue. Lastly, we also tested rabbit ear bleeding model to prove the hemostasis effects on the blood vessels (vein and artery of rabbit ear). The aim of ear bleeding model test was to validate the enhanced hemostatic features of a combination of 532 and 980 nm wavelengths on *in vivo* tissue coagulation.

3.2. Dual mode device design

A new device (**Figure 8.**) was designed to enhance convenience and exactitude in animal experiments. Two fibers were tilted at 23° and -23° for 532 and 980 nm same as *ex vivo* test. The middle of the device created a space to supply the saline. By attaching a support to the device, the distance between the fiber tip and the tissue was fixed.

Figure 8. New designed device for dual-wavelength laser testing in *in vivo* experiment.

3.3. Hemostatic effect of dual-wavelength laser through intentional bleeding in urological tissue

3.3.1. bleeding model of kidney

In vivo experiments were performed on 2-months old female New Zealand white (NZW) rabbit provided from Hana Biotech (Suwon, South Korea). All animal experiments were conducted in accordance with the guidelines of the Korean National Institutes of Health (NIH). The protocol was approved by the Committee on Animal Research at Pukyong National University (Permit Number: 2016-15). Prior to the testing, each rabbit was anesthetized by injecting a zoletil into the muscle. The rabbits were undergoing laparotomy with surgical instruments and covered with sterile cover to show only the kidney (**Figure 9**). 1.5 mm biopsy punch (Disposable biopsypunch, Kai medical, Seki City, Japan) was used for making artificial bleeding in the kidney.

3.3.2. *in vivo* photocoagulation effects on bleeding model

During test, saline was constantly supplied at 4.4 ml/min to the irradiated spot same as *ex vivo* test. Working distance of 3 mm and beam diameter of 1.5 mm were selected for the current study. The tested power condition for 532 and 980 nm were 20 and 40 W. Three different irradiation modes were tested: 532 nm only, 980 nm only, and simultaneous irradiation 532 and 980 nm (dual-wavelength). After the laser treatment, the top surface of each sample was imaged by using a digital camera for checking

photocoagulation effects. Each treated tissue was then fixed in formalin for histological analysis. All the histology slides were stained with hematoxylin and eosin to assess the extent of the irreversible thermal coagulation in the kidney tissue. Image J (National Institute of Health, Bethesda, MD) was then used to detect the coagulation area from the histology. From each histology slide, the coagulation depth and width were defined as the distance between top and bottom of the coagulated area and the overall spatial extent of the coagulated region at the surface.

Figure 10 showed simulation model for the numerical analysis. Kidney tissue was used for tissue model with specific optical properties and prepared in size 30 X 30 X 20 mm. In order to theoretically validate thermal effect of various irradiation conditions on tissue, simple numerical simulations were performed by using a bioheat transfer equation and damage integral. During the laser irradiation, heat transport within the tissue was described by using a bioheat transfer equation as follows:

$$\rho c \frac{\partial T(r,t)}{\partial t} = \nabla \cdot \left(k \nabla T(r,t) \right) + Q_{source}$$

Where ρ (kg/m^3), c ($J/kg{\cdot}K$), and k ($W/m{\cdot}K$) are density, specific heat, and thermal conductivity of the kidney tissue, T (K) the local tissue temperature, and Q_{source} (W/m^3) the heat source associated with light absorption.

Thermal damage was quantified by using a single parameter, Ω that was calculated from the Arrhenius equation.

$$\Omega(\mathrm{r,t}) = A \int_0^t \exp\left[-\frac{\Delta E}{RT(r,t')} \right] dt'$$

26

Where A ($1/s$), ΔE (J/mol), R ($J/mol \cdot K$), T (K), and t are the frequency factor, denaturation activation energy, universal gas constant, absolute temperature in tissue, and the duration of laser irradiation. $\Omega = 1$ represents the extent of the irreversible thermal damage.

3.3.3. Statistical analysis

For statistical analysis (unpaired data), Mann Whitney U test was performed as a non-parametric method on all the measured coagulation depth, width, and volume, and $p <$ 0.05 represents statistical significance.
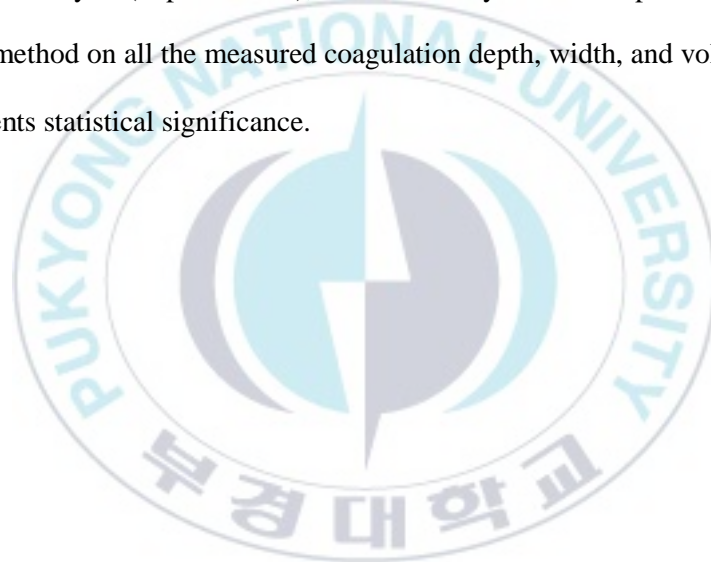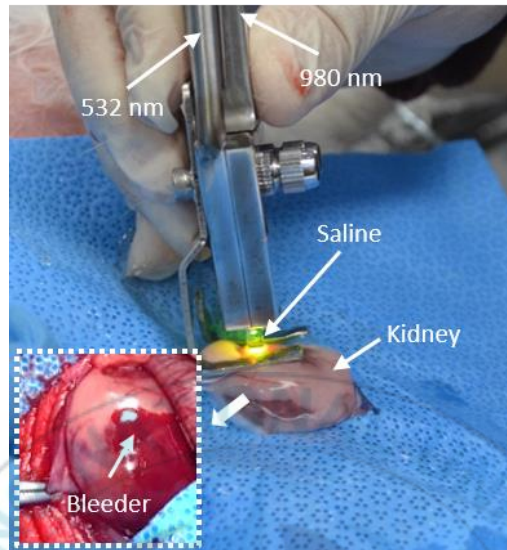
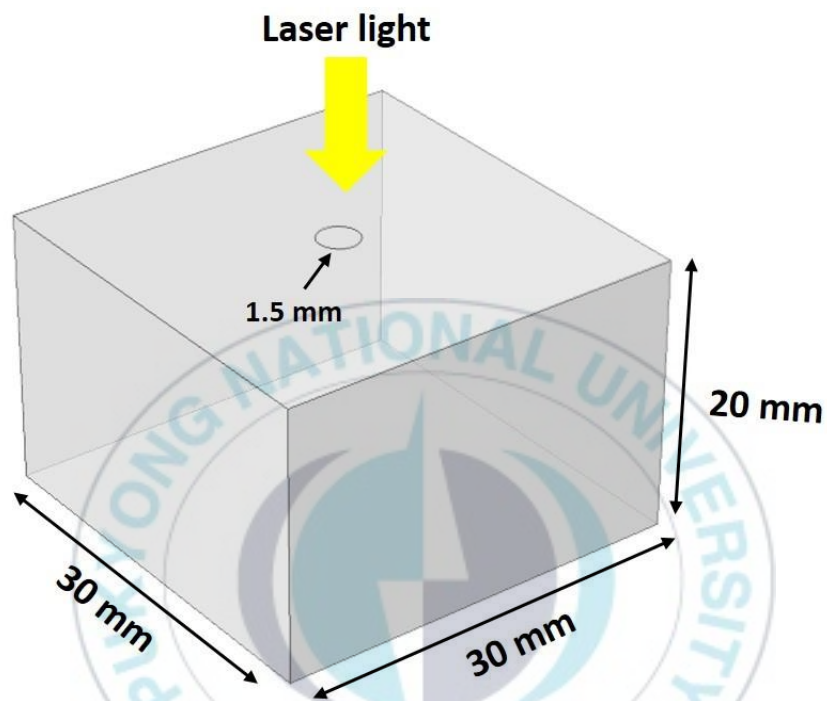Figure 9. Experimental set-up for dual-wavelength hemostasis on kidney tissue

Figure 10. Numerical simulation set-up for dual-wavelength photocoagulation on kidney tissue.

3.4. Results and Discussion (urological tissue)

3.4.1. Photocoagulation effects in kidney tissue

Figure 11A showed surface images of porcine kidney tissue after laser coagulation. The white region represent coagulation necrosis (CN) effects that is a type of accidental cell death. Carbonization (CB) effects was irreversible reaction where cells and tissue were destroyed over 200 ℃. CN effects were occurred in all conditions after laser irradiation. However, 532 nm after laser irradiation was made CB unlike dual-wavelength. **Figure 11B** presented coagulation time that could stop bleeding by laser irradiation. Initially, significant bleeding was confirmed at the wound site prior to laser irradiation. However, 4 seconds after the irradiation, the disappearance of bleeding vividly evidenced that the application of the dual-wavelength eventually achieved the complete hemostasis. Also, 980 nm was occurred hemostasis after 12.8±8.1 second but it wasn't always stopped bleeding. Compare with between 980 nm and dual-wavelength, coagulation time of dual-wavelength showed 3 times shorter ($P < .001$). The 532 nm couldn't stopped the bleeders completely as the bleeding continued at the wound. Therefore, these results indicated that dual-wavelength could stop bleeding more the faster and effective than other conditions.
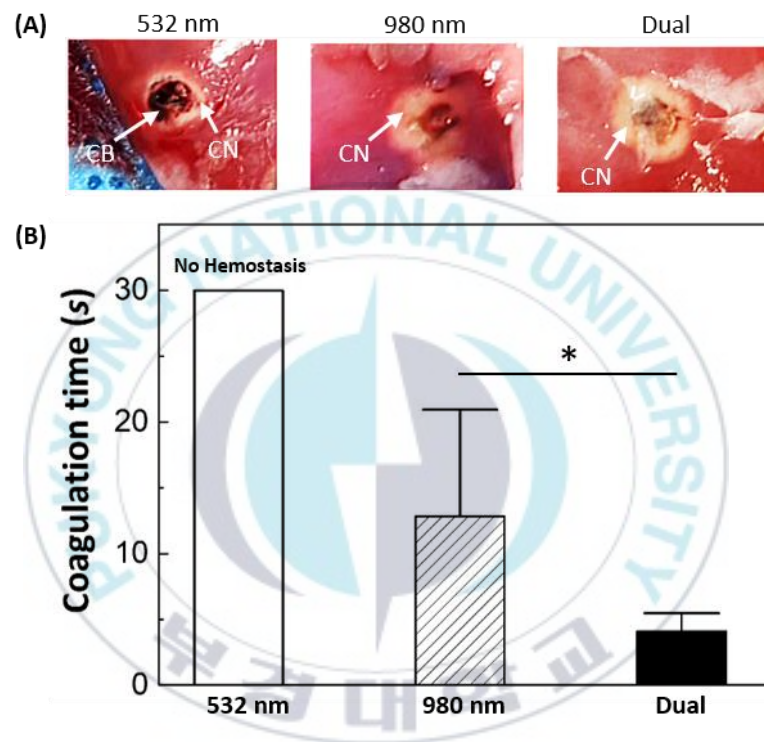
Figure 11. Hemostatic effect depending on irradiation modes: (A) surface images of coagulated tissue and (B) coagulation time.

3.4.2. Histological analysis

Figure 12A exhibited histological images after photo-thermal coagulation (top: 10x, bottom: 40x). Coagulation area of 980 nm and dual were showed similar area unlike 532 nm. After laser irradiation, transformed cells and blood clot inside the tissue were observed in all conditions. The degree of the tissue coagulation for all the tested conditions was quantified from histology images shown in **Figure 12B**. The dual wavelength irradiation entailed deeper and wider coagulation than the 532 nm did (depth: $P = .03$, width: $P = .004$), but a similar coagulation depth and width to that of the 980 nm (depth: $P = .3$, width: $P = .7$). Despite of the long laser irradiation time, the 532 nm produced less coagulation area than both 980 nm and dual-wavelength. In numerical simulation, although short irradiation time, the dual-wavelength showed almost similar temperature distribution and thermal distribution. In in vivo test and numerical simulation, the dual-wavelength was confirmed effective thermal coagulation after laser irradiation.
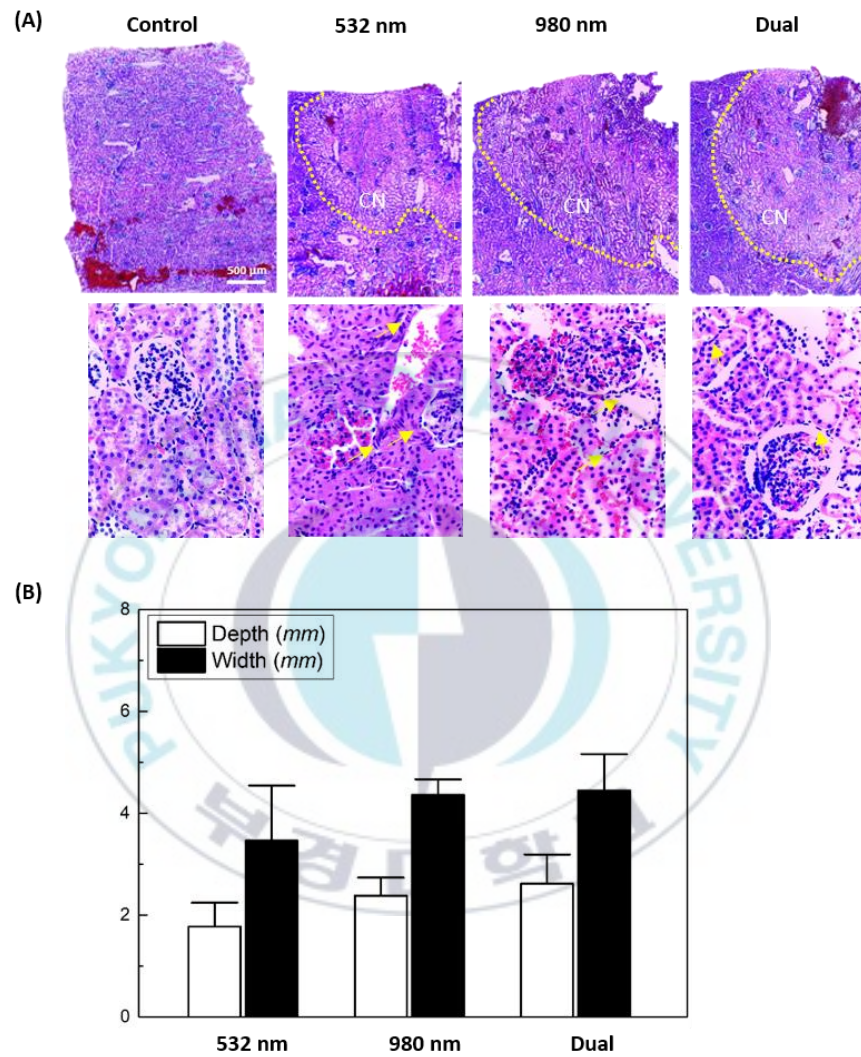
Figure 12. H&E stained histological images of kidney tissue: (A) Histology (top:10x and bottom:40x) and (B) measured coagulation

3.5. Hemostatic effect of dual-wavelength laser according to blood pressure in ear tissue

3.5.1. bleeding model of ear

In vivo experiments were performed on 2-months old female New Zealand white (NZW) rabbit provided from Hana Biotech (Suwon, South Korea). All animal experiments were conducted in accordance with the guidelines of the Korean National Institutes of Health (NIH). The protocol was approved by the Committee on Animal Research at Pukyong National University (Permit Number: 2017-33). Prior to the testing, each rabbit was anesthetized by injecting a zoletil into the muscle. Then, the back of each rabbit was shaved with a clipper. Two different blood vessels were evaluated for hemostasis possibility according to laser condition: vein vessels and artery vessels (**Figure 13**). Prior to the testing, 1.5 mm biopsy punch (Disposable biopsypunch, Kai medical, Seki City, Japan) was used for making artificial bleeding in the rabbit ear.

3.5.2. *in vivo* photocoagulation effects on bleeding model

Figure 14 showed experiment set-up for hemostasis using hand-held device with dual-wavelength. During the test, saline was constantly supplied at 4.4 ml/min to the irradiated spot like *ex vivo* test. Working distance of 3 mm and beam diameter of 1.5 mm were selected for the current study. The tested power condition for 532 and 980

nm were 20 and 40 W. Three different irradiation modes were tested: 532 nm only, 980 nm only, and simultaneous irradiation 532 and 980 nm (dual-wavelength). For group 1 (vein vessel) and group 2 (artery vessel), three different irradiation modes were observed hemostasis effects at 0 to 4 weeks. To estimate physical variations in the wound size, the wounded area of each group were photographed every 1 weeks. To observe histological changes, rabbits were euthanized at 0, 1, 2, 3 and 4 weeks. Each treated tissue was then fixed in formalin and prepared for histological analysis. All the histology slides were stained with hematoxylin and eosin to assess the extent of the irreversible thermal coagulation in ear tissue. All the prepared slides were observed under an optical microscope.
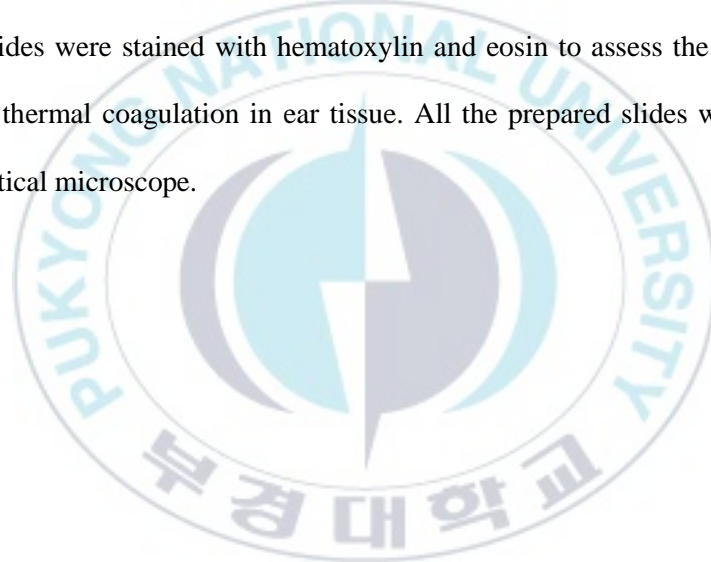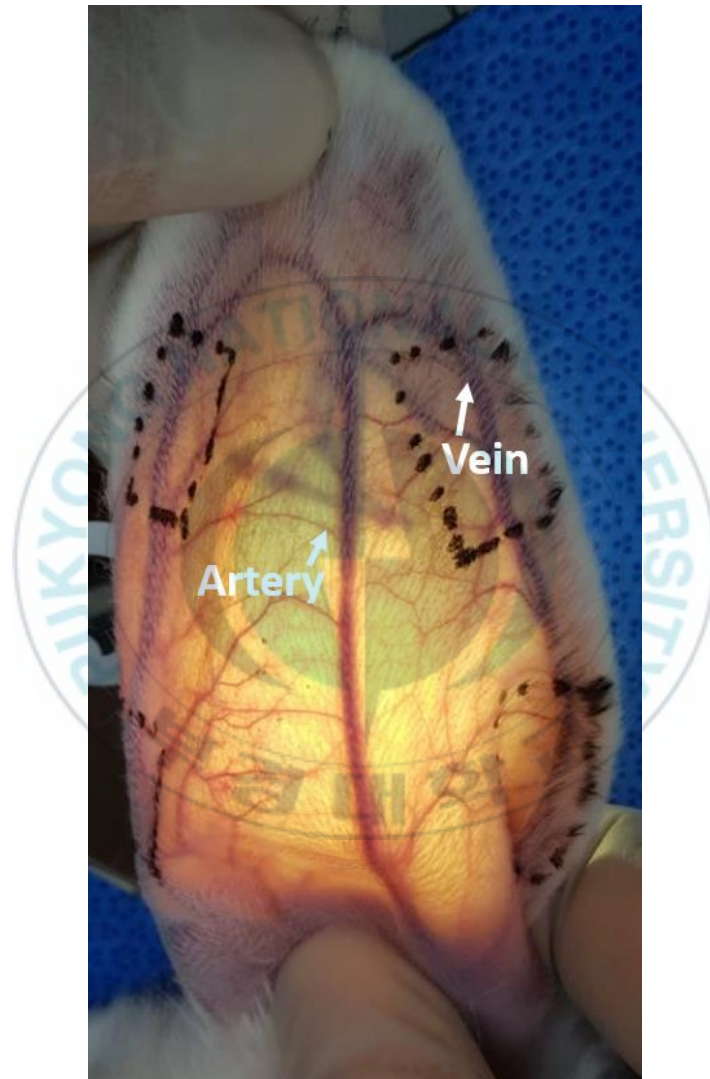
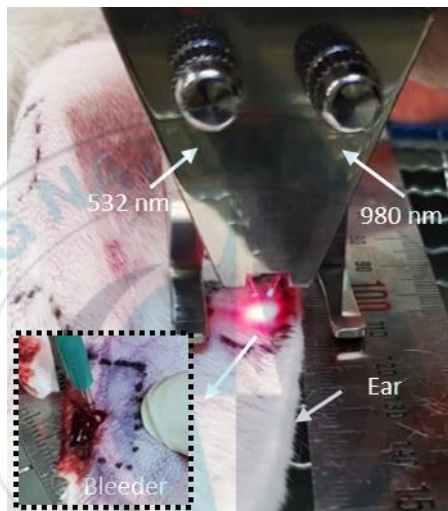Figure 13. Confirmation of vein and artery vessels in rabbit ear

Figure 14. Experimental set-up for hemostasis effects depending on the blood vessels

3.6. Results and Discussion (Ear tissue)

3.6.1. Photocoagulation effects in ear

To monitor progress of wound healing, the wounded regions of all groups were photographed at various time points (**Figure 15A and Figure 16A**). Overall, the wound size of all the groups decreased with the healing time. Immediately after injury (day 0), the initial wound size were different for all groups. Compare with group 1 at day 0, carbonizations were observed at day 0 in group. After 1 week, all groups suffered from swelling around wound by inflammatory response. Later, the wound size of group 1 dramatically was decreased and created a scar. Also, the wound size of group 2 was decreased after 3 weeks and created a scar. **Figure 15B** and **Figure 16B** presented coagulation time that was stopped bleeding by laser irradiation. In Group 1 (**Figure 15**), coagulation time of the two single wavelengths (532 nm and 980 nm) showed similar time. However, in Group 2 (**Figure 16**), coagulation time of 980 nm was longer than that of 532 nm. The application of the dual-wavelength eventually achieved the complete hemostasis after 3 seconds in group1 and 2. On the other hand, 532 and 980 nm could not stop the bleeding from the wound. In these results, dual-wavelength could achieve hemostasis faster and more effective than other conditions like previous in vivo kidney test.

3.6.2. Histological analysis

Figure 17 showed histological image after photo-thermal treatment. After laser irradiation, blood vessels of both vein and artery were changed by laser light. In all conditions except control, the homogeneous dermal collagen was discovered due to thermal injury after thermal treatment at 0 day. Hemorrhage was observed in all groups in 1 week, and inflammatory reactions was confirmed within 2 weeks. As a results, vascular deformation and inflammatory responses by photo-thermal were observed in all groups.
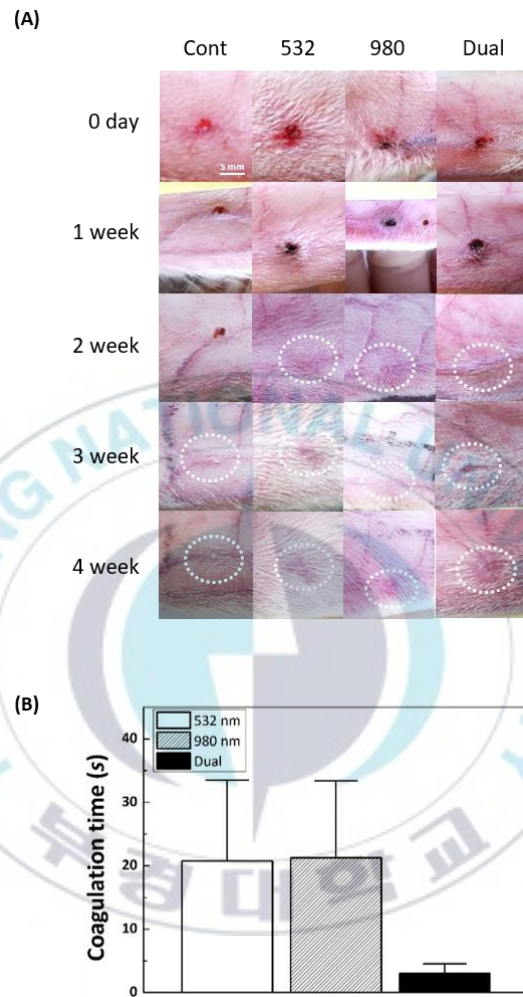
Figure 15. Top view images of lesions on weeks 0, 1, 2, 3 and 4 after treatment: (A)
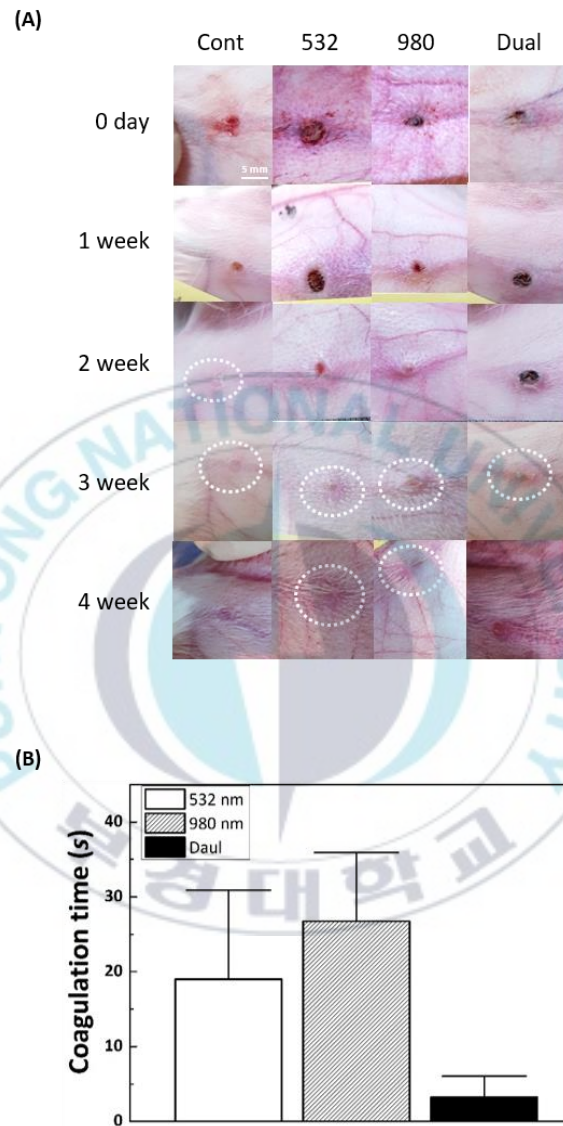
Group 1: vein and (B) coagulation time

Figure 16. Top view images of lesions on weeks 0, 1, 2, 3 and 4 after treatment: (A) Group 2: artery and (B) coagulation time
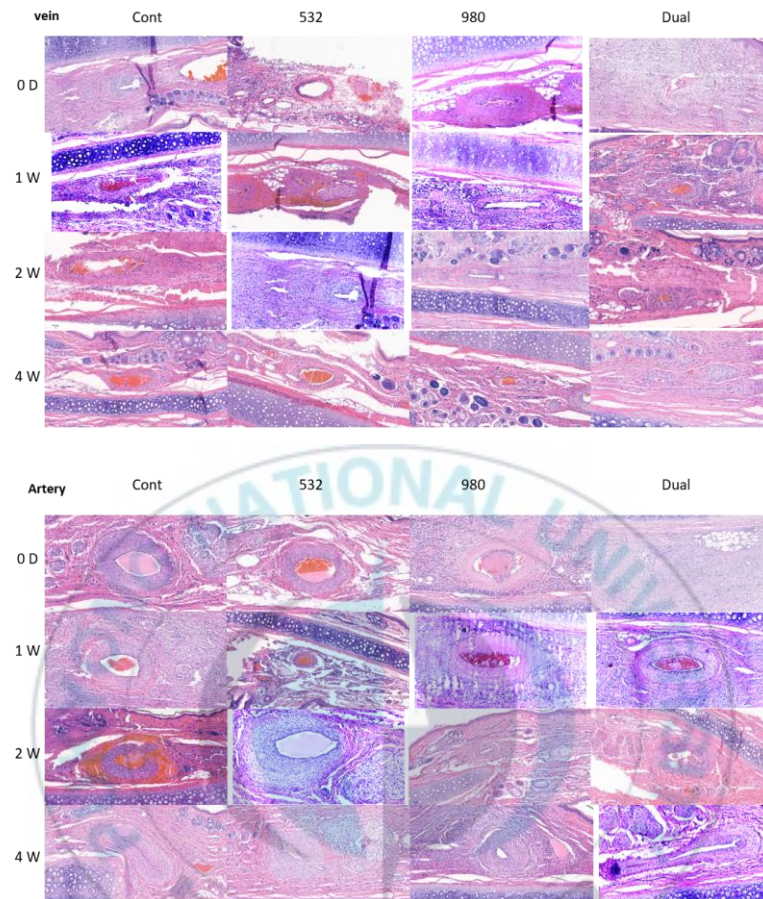
Figure 17. Hematoxylin and eosin stained histological images of damaged tissue for vein and artery in the ear

4. Discussion

The goal of research was to investigate feasibility and treatment efficacy of dual wavelengths laser for effective hemostasis in BPH treatment. As each wavelength is associated with different optical penetrations in blood and soft tissue [25], the simultaneous irradiation of two wavelengths (532 and 980 nm) could contribute to the enhancement of coagulation (**Figures 3 and 4**). In turn, the resultant thermal augmentation with a larger coagulation volume (**Figure 4(b)**) could accompany rapid and complete thermal hemostasis by achieving a deep and wide range of the coagulative coverage on the bleeding sites (**Figure 6**). In spite of delivery of higher total power (60 W = 20 W for 532 nm + 40 W for 980 nm) to the bleeders, no considerable tissue ablation was observed in both kidney tissues and skin phantoms during the experiments. Hence, the dual-wavelengths with different optical characteristics could additively induce heat accumulation and augment the spatial extent of the irreversible thermal coagulation on the bleeding sites, possibly leading to the complete hemostasis for the laser prostatectomy.

According to numerical simulations (**Figure 7**), dual-wavelength with higher laser power yielded a surface temperature 52 and 42% higher than 532 and 980 nm wavelengths did, respectively. The increased surface temperature along with the wavelength-dependent tissue responses (i.e., absorption and scattering) resulted in an ostensibly deeper and wider area, which is congruent with the overall trend from the

current experimental results (**Figures 3 and 4**). However, the detailed discrepancy between the simulation and the experimental results still exist possibly due to partial phase change of tissue, convective cooling, and variations in tissue properties. Hence, an in-depth numerical analysis should be performed to elucidate the collective thermal effects of the dual-wavelength on tissue coagulation and hemostasis by taking into account the changes in optical and thermal properties, surface convection by saline cooling, micro-pulse schemes, and dynamic fiber movements (i.e., moving heat source) during the irradiation [**23**, **26**,**27**].

As 2 different fibers were employed to deliver 532 and 980 nm wavelengths in *ex vivo* test, hand-held device was designed to enhance for convenience and exactitude during *in vivo* test (**Figure 8**). For developing the bleeding model in *in vivo* test, two type of bleeding model (kidney and ear) were selected to check the hemostasis possibility using dual-wavelength (**Figure 9 and Figure 14**). Also, the kidney and ear model of rabbit were not related to the prostate, but it was used to identify the hemostasis possibility that demonstrated in *ex vivo* test. As the kidney has many small vessels among the urological tissue, it is effective to create the bleeding model. So, we studied the possibility of hemostasis using dual-wavelength laser in kidney bleeding model. As a results, in *in vivo* kidney experiment as well as *ex vivo* experiment, dual-wavelength were able to identify faster and more effective hemostasis effect (**Figure 11 and Figure 12**). In case of 532 nm, despite longer laser irradiation time than other conditions, 532 nm could not stop the bleeding completely in the same with *ex vivo* test. However, *in vivo* kidney test was difficult in proving possibility of hemostasis to arterial bleeding.

44

During BPH procedure, the arterial bleeding is big problem due to obstruct surgeon's view. So, various blood vessels were estimated hemostasis effects in terms of chronic response and wound healing before clinical study. The rabbit ears were used to evaluate hemostasis possibility depending on the vessels (vein and artery). In in vivo ear test, dual-wavelength achieved the complete hemostasis in all of conditions (vein and artery) (**Figure 15 and Figure 16**). Overall results of study, dual-wavelength laser showed complete hemostasis in all bleeding situations.

Although the current study demonstrated the feasible hemostatic capability of dual-wavelength due to the augmented thermal effects, experimental limitations still remain in order to translate the proposed technique into clinical situations. As 2 fibers were employed to deliver 532 and 980 nm wavelengths in the study, the simultaneous transmission of the dual wavelength still needs to be examined in a single device. Current device for *in vivo* testing was still big and inappropriate to insert inside the prostate. For clinical testing, an optical beam combiner will be designed and development to transmit the dual-wavelength in a single optical fiber. Thus, further studies are underway to perform canine prostate testing to explore the effectiveness of the dual-wavelength irradiation on bleeding control during in vivo laser prostatectomy [5].

5. Conclusion

In the present study, both ex vivo and in vivo assessments were performed to investigate the photocoagulation effects of dual-wavelength laser in the bleeding model. The dual wavelength showed rapid procedure time and a complete hemostatic effect. The combined wavelengths accompanied more extensive lateral heat diffusion as well as deeper optical penetration. Therefore, the dual-wavelength assisted coagulation can be a feasible treatment to entail the rapid hemostasis in an effective manner.
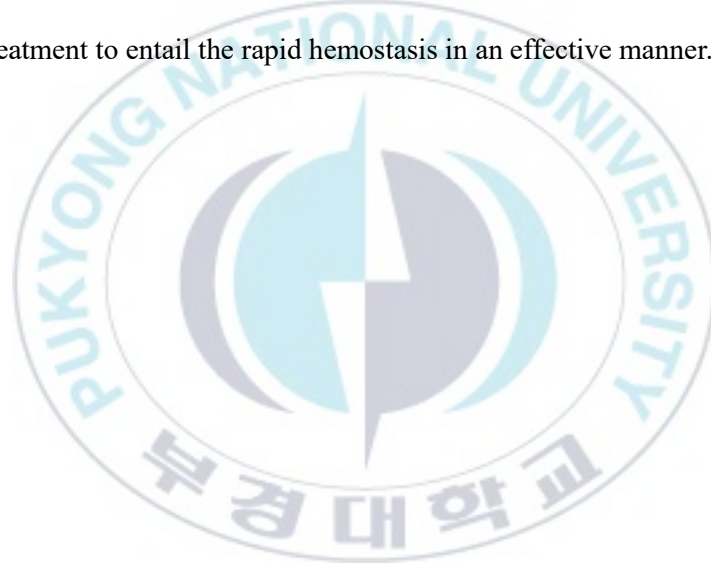
6. References

[1] A. Bachmann, A. Tubaro, N. Barber, F. d'Ancona, G. Muir, U. Witzsch, M.-O. Grimm, J. Benejam, J.-U. Stolzenburg, A. Riddick, S. Pahernik, H. Roelink, F. Ameye, C. Saussine, F. Bruyère, W. Loidl, T. Larner, N.-K. Gogoi, R. Hindley, R. Muschter, A. Thorpe, N. Shrotri, S. Graham, M. Hamann, K. Miller, M. Schostak, C. Capitán, H. Knispel, and J. A. Thomas, *Eur. Urol.* **65**, 931-942 (2014).

[2] R. Unnikrishnan, N. Almassi, and K. Fareed, *Cleve. Clin. J. Med.* **84**, 53-64 (2017).

[3] S. Gravas, A. Bachmann, O. Reich, C. G. Roehrborn, P. J. Gilling, and J. De La Rosette, *BJU Int.* **107**, 1030-43 (2011).

[4] S. M. Nair, M. A. Pimentel, and P. J. Gilling, *Curr. Urol. Rep.* **17**, 45 (2016).

[5] R. S. Malek, H. W. Kang, Y. S. Peng, D. Stinson, M. T. Beck, and E. Koullick, *J. Urol.* **185**, 712-8 (2011).

[6] A. Bachmann, G. H. Muir, E. J. Collins, B. B. Choi, S. Tabatabaei, O. M. Reich, F. Gomez-Sancha, and H. H. Woo, *Eur. Urol.* **61**, 600-7 (2012).

[7] B. Choi, S. Tabatabaei, A. Bachmann, E. Collins, J. de la Rosette, F. Gómez Sancha, G. Muir, O. Reich, and H. Woo, *Eur. Urol. Suppl.* **7**, 384-392 (2008).

[8] K. C. Zorn and D. Liberman, *Can. J. Urol.* **18**, 5918-26 (2011).

[9] D. S. Elterman, *Can. J. Urol.* **22**, 7836-43 (2015).

[10] P. Castellan, R. Castellucci, L. Schips, and L. Cindolo, *World J. Urol.* **33**, 599-607 (2015).

[11] C. P. Swain, S. G. Bown, D. W. Storey, J. S. Kirkham, T. C. Northfield, and P. R. Salmon, *Lancet* **2**, 1313-6 (1981).

[12] T. R. Viggiano, J. Zighelboim, D. A. Ahlquist, C. J. Gostout, K. K. Wang, and M. V. Larson, *Gastrointest. Endosc.* **39**, 513-7 (1993).

[13] O. Reich, A. Bachmann, P. Schneede, D. Zaak, T. Sulser, and A. Hofstetter, *J Urol* **171**, 2502-4 (2004).

[14] J. K. Anderson, M. R. Baker, G. Lindberg, and J. A. Cadeddu, *Eur Urol* **51**, 749-54 (2007).

[15] C. M. Cilip, S. B. Rosenbury, N. Giglio, T. C. Hutchens, G. R. Schweinsberger, D.

Kerr, C. Latimer, W. H. Nau, and N. M. Fried, *J Biomed Opt* **18**, 58001 (2013).

[16] N. C. Giglio, T. C. Hutchens, W. C. Perkins, C. Latimer, A. Ward, W. H. Nau, and N. M. Fried, *J Biomed Opt* **19**, 38002 (2014).

[17] C. M. Cilip, D. Kerr, C. A. Latimer, S. B. Rosenbury, N. C. Giglio, T. C. Hutchens, W. H. Nau, and N. M. Fried, *Lasers Surg Med* **49**, 366-371 (2017).

[18] M. Rieken, H. W. Kang, E. Koullick, G. R. Ruth, and A. Bachmann, *Lasers Surg Med* **42**, 736-42 (2010).

[19] L. Aaron, O. E. Franco, and S. W. Hayward, *Urol Clin North Am* **43**, 279-88 (2016).

[20] F. A. Duck, Physical Properties of Tissues, (Academic Press, London, 1990), pp. 9-43.

[21] R. Patnaik and R. N. Padhy, *Interdiscip Toxicol* **8**, 35-43 (2015).

[22] T. H. Nguyen, S. Park, K. K. Hlaing, and H. W. Kang, *Biomed. Opt. Express* **7**, 1932-47 (2016).

[23] M. H. Niemz, Laser-tissue Interactions: Fundamentals and Applications, (Springer-Verlag, Berlin, 2004), pp.

[24] M. Mesradi, A. Genoux, V. Cuplov, D. Abi Haidar, S. Jan, I. Buvat, and F. Pain, *J Biomed Opt* **18**, 117010 (2013).

[25] J. P. Ritz, A. Roggan, C. T. Germer, C. Isbert, G. Muller, and H. J. Buhr, *Lasers Surg Med* **28**, 307-12 (2001).

[26] S. C. Jiang and X. X. Zhang, *Lasers Med Sci* **20**, 122-31 (2005).

[27] J. Oh, S. Y. Nam, Y. W. Lee, and H. W. Kang, *Lasers Surg. Med.* **48**, 616-23 (2016).

Acknowledgment